Online Research @ Cardiff

This is an Open Access document downloaded from ORCA, Cardiff University's institutional repository: https://orca.cardiff.ac.uk/id/eprint/144158/

This is the author's version of a work that was submitted to / accepted for publication.

Citation for final published version:

Ungerer, Marietjie J. ORCID: https://orcid.org/0000-0002-9073-1186, Santos Carballal, David ORCID: https://orcid.org/0000-0002-3199-9588, De Leeuw, Nora H. ORCID: https://orcid.org/0000-0002-8271-0545 and van Sittert, Cornelia 2021. Competitive adsorption of H2O and SO2 on catalytic platinum surfaces: a density functional theory study. South African Journal of Chemistry 74 (1) , pp. 57-68. 10.17159/0379-4350/2020/v74a00 file

Publishers page: https://doi.org/10520/ejc-chem-v74-nse1-a10 <https://doi.org/10520/ejc-chem-v74-nse1-a10>

Please note:
Changes made as a result of publishing processes such as copy-editing, formatting and page numbers may not be reflected in this version. For the definitive version of this publication, please refer to the published source. You are advised to consult the publisher's version if you wish to cite this paper.

This version is being made available in accordance with publisher policies. See http://orca.cf.ac.uk/policies.html for usage policies. Copyright and moral rights for publications made available in ORCA are retained by the copyright holders.

information services
gwasanaethau gwybodaeth

Competitive Adsorption of H_2O and SO_2 on Catalytic Platinum Surfaces: A Density Functional Theory Study

Marietjie J. Ungerer,[1,2] David Santos-Carballal,[2,3]
Cornelia G. C. E. van Sittert *[1] and Nora H. de Leeuw *[2,4]

[1] Laboratory for Applied Molecular Modelling, Research Focus Area: Chemical Resource Beneficiation, North-West University, Private Bag X6001, Potchefstroom, 2520, South Africa

[2] School of Chemistry, Cardiff University, Main Building, Park Place, Cardiff CF10 3AT, United Kingdom

[3] Materials Modelling Centre, School of Physical and Mineral Sciences, University of Limpopo, Private Bag X1106, Sovenga 0727, South Africa

[4] Department of Earth Sciences, Utrecht University, Princetonplein 8A, 3584 CD Utrecht, The Netherlands

[*Corresponding Authors E-mails: Cornie.VanSittert@nwu.ac.za; N.H.DeLeeuw@uu.nl]

Abstract

Platinum has been widely used as the catalyst of choice for the production of hydrogen in the hybrid sulphur (HyS) cycle. In this cycle, water (H_2O) and sulphur dioxide (SO_2) react to form sulphuric acid and hydrogen. However, the surface reactivity of platinum towards H_2O and SO_2 is not yet fully understood, especially considering the competitive adsorption that may occur on the surface. In this study, we have carried out density functional theory calculations with long-range dispersion corrections [DFT-D3-(BJ)] to investigate the competitive effect of both H_2O and SO_2 on the Pt (001), (011), and (111) surfaces. Comparing the adsorption of a single H_2O molecule on the various Pt surfaces, it was found that the lowest adsorption energy (E_{ads} = −1.758 eV) was obtained for the dissociative adsorption of H_2O on the (001) surface, followed by the molecular adsorption on the (011) surface (E_{ads} = −0.699 eV) and (111) surface (E_{ads} = −0.464 eV). For the molecular SO_2 adsorption, the trend was similar, with the lowest adsorption energy (E_{ads} = −2.471 eV) obtained on the (001) surface, followed by the (011) surface (E_{ads} = −2.390 eV) and (111) surface (E_{ads} = −1.852 eV). During competitive adsorption by H_2O and SO_2, the SO_2 molecule will therefore preferentially adsorb onto the Pt surface. If the concentration of SO_2 increases, self-reaction between two neighbouring SO_2 molecules may occur, leading to the formation of sulphur monoxide (SO) and -trioxide (SO_3) on the surface, which could lead to sulphur poisoning of the Pt catalytic surface.

Keywords: Platinum, Water, Sulphur Dioxide, Hydrogen, Adsorption, Density Functional Theory

1. Introduction

The increasing demand to reduce toxic emissions, not only from automotive engines [1], but also for example in the aviation sector [2], steel manufacturing and electricity generation,[3] has driven extensive research toward the production of clean, renewable and sustainable energy, e.g. from wind [4,5], solar,[6–8] hydroelectricity [9,10] or combinations thereof [11–13], or alternative energy sources such as hydrogen (H_2).[14] Currently, various different feedstocks are used for the production of H_2 [15], including from biomass [16], nuclear [17] or waste water [18], the non-carbon-based hybrid sulphur (HyS) cycle which has shown itself as a promising, potentially large-scale process.[19,20] During the HyS cycle, sulphur dioxide (SO_2)/sulphuric acid (H_2SO_4) is used in an electro-oxidation reaction, leading to the net reaction of splitting the water (H_2O) into H_2 and oxygen (O_2). Various anode catalysts [20] have been tested for this reaction and the carbons supported metallic platinum (Pt) catalysts has consistently shown both high activity and stability [21–23] towards this reaction.

Sulphur-containing molecules, including SO_2, SO and S, have long been known to be among the key poisoning compounds in heterogeneous catalysis.[24] As such, one of the major problems with Pt anode catalysts is the formation of a sulphur (S) layer on the surface, leading to catalyst poisoning, i.e. deactivation and in severe cases surface delamination.[25,26] Despite their acknowledged role in the poisoning of these supported Pt metal catalysts,[26] the fundamental chemistry and mechanistic behaviour of the sulphur-metal interaction remains poorly defined. To understand the deactivation mechanism on a fundamental level, some experimental and theoretical studies focussed on SO_2 adsorption on various Miller indexes of pure metal surfaces, including Cu [27–30], Ni [31–33], Ag [34,35], Rh [36,37], Pd [29,37–41], and Pt [29,36,42–45]. Although Pt is the most studied system, opposing results have been obtained for SO_2 adsorbed onto the Pt (111) surface.[24] This is due to the operational conditions, e.g. surface coverage and surface morphology, during the SO_2 oxidation/reduction reactions, influencing the thermodynamics leading to different final products.[46] However, major difficulties have been experienced in experiments, because even when pure sulphur oxides, such as SO_2, were adsorbed from the gas phase onto single metallic catalysts, a number of co-adsorbed sulphur species were detected on the surface. [47–49] Moreover, very little theoretical work or modelling has been performed on evaluating the reaction energies and thermodynamics of these sulphur oxides with the various Pt surfaces.

Pt is widely used in various reactions in which water acts both as a participant or bystander, [50] influencing the behaviour of the heterogeneous catalytic surface.[51] The nature of the H_2O–metal interaction is of obvious importance [52,53] and considerable research effort has been devoted towards understanding these systems.[54–56] A major challenge in modelling the adsorption of water on a catalytic surface are the multitude of atomic position variations in the simulated liquid, which necessitates the addition of several different configurations [56,57] in the initial computational set up. Previous

modelling studies showed [58,59] that the most reliable results extensively looked at the way the water molecules interacts with each other and the surface and does not necessitate adsorption of additional water molecules onto the surface. Another factor to consider is the splitting of the water molecule into H^+ + OH^- and how these species affect not only the catalytic surface, but also the behaviour of co-adsorbed species. It is evident that the detailed description of the binding behaviour of water molecules onto Pt surfaces is still not complete. The starting point here will be an in-depth understanding of the behavior between the H_2O molecules and the metal surface atoms.

In this paper, we have used DFT calculations to predict the behavior of H_2O and SO_2 on the electro-catalytically active surfaces of platinum metal, i.e. the Pt (001), (011), and (111) surfaces. We examine the adsorption energy of various geometries, any charge transfer between the Pt surface and the adsorbates as well as the work function. The overall aim of our study was the development of a comprehensive understanding of the H_2O-surface and SO_2-surface chemistry on the electro-catalytically active surfaces of Pt, and in particular the competition between these two reactants in the HyS cycle for specific surface adsorption sites, which will be the initial step in the overall HyS reaction process.

2. Computational Methods

2.1 Surface Calculation Details

The Vienna Ab Initio Simulation Package (VASP) [60–63] has been shown to give accurate surface adsorption data [64–67] and was therefore used to simulate the Pt surfaces and their interactions with H_2O [68] and SO_2 [69]. The projector augmented wave (PAW) [70,71] method was employed to describe the interaction between the valence and the core electrons. The core electrons of Pt were defined up to and including the 5p orbitals. The Perdew, Burke and Ernzerhof (PBE) [72,73] functional within the generalised gradient approximation (GGA) was applied in all calculations. Plane-waves were included to a cut-off of 400 eV. The long-range dispersion interactions were considered with the DFT-D3 method with Becke-Johnson (BJ) damping.[74] The Methfessel-Paxton scheme order 1 [75] was used with a smearing of 0.05 eV to determine the partial occupancies during geometry optimisation, ensuring an electronic entropy of less than 1 meV.atom^{-1}. However, the tetrahedron method with Blöchl corrections [76] was used in the final static simulations to obtain accurate total energies and charges. The electronic and ionic optimisation criteria were 10^{-5} eV and 10^{-2} eV. Å^{-1}, respectively, and the conjugate gradient technique was adopted for the geometry optimisations.

Pt has a $Fm\bar{3}m$ crystal structure [77] and the bulk Pt structure was calculated within a primitive face-centred cubic (*fcc*) cell using a *Γ*-centred 17 x 17 x 17 Monkhorst-Pack [78] *k*-point mesh. Previous work has shown that long-range dispersion approximations influence not only the lattice parameters of a modelled surface, but also its surface energy.[64,68] In this paper the geometry optimisation of the Pt

(001), (011) and (111) surfaces have therefore been carried out with the DFT-D3(BJ) method.[74] Our calculated *fcc* Pt lattice constant was 3.926 Å, which is in excellent agreement with the experimental value of 3.924 Å.[79,80]

The Pt (001), (011) and (111) surfaces were investigated by simulating the periodic p(3 x 3), p(3 x 3) and p(4 x 4) supercells, respectively, which were generated from the bulk using the METADISE code [81]. A vacuum of 15 Å was added in the *z*-direction perpendicular to the plane of the surface, to avoid interaction between the neighbouring cells. Each slab contained four atomic layers and the surface areas of the supercells were 138.17 Å^2, 196.18 Å^2 and 106.79 Å^2 for the (001), (011) and (111) surfaces, respectively. The atoms in the two bottom layers of the slabs were fixed in the optimised bulk positions and the atoms in the remaining two layers were allowed to relax freely. A *Γ*-centred 7 x 7 x 1 Monkhorst-Pack *k*-point grid was used for all the surface systems to sample the Brillouin zone.

The unrelaxed (γ_u) and relaxed (γ_r) surface energies were determined using equations (1) and (2), respectively:

$$\gamma_u = \frac{E_{slab,u} - N_{Pt,slab}E_{Pt,bulk}}{2A_{slab}} \quad (1)$$

$$\gamma_r = \frac{E_{slab,r} - N_{Pt,slab}E_{Pt,bulk}}{A_{slab}} - \gamma_u \quad (2)$$

where $E_{slab,u}$,$E_{slab,r}$ and $E_{Pt,bulk}$ are the energies of the unrelaxed slab, the half-relaxed slab and the bulk, respectively. $N_{Pt,slab}$ and A_{slab} represent the number of Pt atoms in the slab and the surface area of the slab, respectively. The percentage relaxation (R) was calculated as the difference between the unrelaxed and relaxed surface energies, divided by the unrelaxed surface energy and multiplied by 100.

The work function (Φ) is the minimum energy needed to remove an electron from the bulk of a material through a surface to a point outside the material. Here, we have calculated the energy needed to remove an electron from the Fermi level (E_f) of the metal surface to the vacuum potential (E_{vac}) at 0 K.[82]

Atomic charges for the pristine surfaces were obtained using Bader analysis, [83–86] which partitions space into non-spherical atomic regions enclosed by local minima in the charge density.

2.2 Adsorption Calculation Details

The isolated H_2O and SO_2 molecules for reference were optimised in periodic boxes of 12 x 13 x 14 Å^3 to ensure negligible interaction with their images in periodically repeated neighbouring cells. The Gaussian smearing scheme [75] was used during geometry optimisation and energy calculations were carried out with a smearing of 0.05 eV. A *Γ*-centred 1 x 1 x 1 Monkhorst-Pack [78] *k*-point mesh was

used. Dipole corrections were added in all directions and the H_2O and SO_2 molecules were computed without symmetry. The core electrons of O and S were defined up to and including the 1s and 2p orbitals, respectively. For the H atoms, all the electrons were treated as valence electrons. Again, the atomic charges for the single molecules and adsorbed systems were obtained using Bader analysis. [83–86]

3. Results and Discussion

In this section we briefly describe the Pt surface slabs with the low Miller indices (001), (011) and (111) (Section 3.1), followed by an overview of the adsorption of both H_2O and SO_2 (Section 3.2), with detailed descriptions of their behaviour on the Pt (001), (011) and (111) surfaces discussed in Sections 3.2.1, 3.2.2 and 3.2.3, respectively.

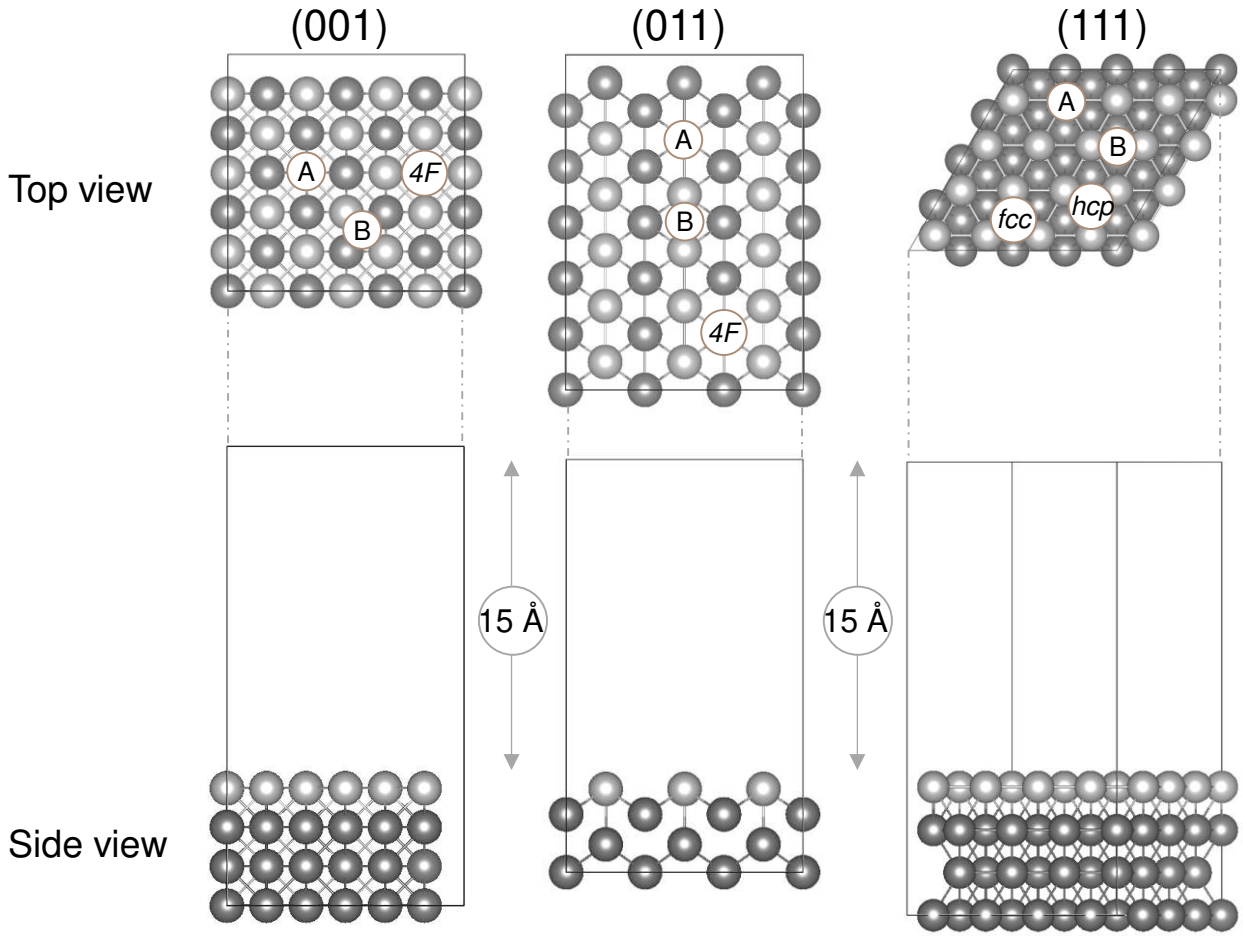

Figure 1 – Top and side views of the Pt (001), (011) and (111) surfaces. The symmetrically inequivalent adsorption sites are indicated, i.e. atop (A), bridge (B), four-fold hollow (4F), hexagonal close packed (*hcp*) and face-centred cubic (*fcc*). The silver colour is used throughout this paper for Pt, with the top layer shown lighter for visualisation purposes.

3.1 Surface Structures

The top and side views of the Pt (001), (011) and (111) surfaces used in our simulations are shown in Figure 1. To distinguish between top layer and subsequent layer atoms, the colour of the atoms in the top layer of each of the surfaces were changed to lighter silver. All three surfaces are planar, bulk-terminated structures, with each slab containing four atomic layers plus a 15 Å vacuum space in the *z*-direction. The Pt (001) and Pt (111) surfaces are smooth with a face-centred cubic arrangement, while the Pt (011) is open-facetted, forming grooves on the surface. The adsorption sites indicated in Figure 1 for the Pt (001) and (011) surfaces are atop (A), bridge (B) and four-fold hollow (4F), while the Pt (111) surface has atop (A), bridge (B), hexagonal close packed (*hcp*) and face-centred cubic (*fcc*) sites.

Table 1 lists the relaxed and unrelaxed surface energies and the surface areas for the Pt (001), (011) and (111) surfaces. In terms of surface energy, our calculations correlated with previously identified trends, where Pt (111) has the lowest surface energy and is hence the most stable plane, followed by the (001) and (011) surfaces. Literature reported an experimental surface energy of 2.48 J/m^2 [87] which is in good (quantitative) agreement with our calculated surface energies, particularly if we keep in mind that our perfect surfaces will lead to smaller surface energies than experimental surfaces, which are bound to contain defects that raise the surface energy.[88]

Table 1 – Unrelaxed (γ_u) and relaxed (γ_r) surface energies, percentage of relaxation (R), the surface areas (A), the work function (Φ) and d-band centre values for the Pt (001), (011) and (111) surfaces.

	Pt (001)[68,69]	Other works	**Pt (011)**[68,69]	Other works	**Pt (111)**[68,69]	Other works
γ_u (J/m^2)	2.472		2.691		2.055	
γ_r (J/m^2)	2.462	1.81 [89], 2.17 [90]	2.615	1.85 [89], 2.37 [91]	2.046	1.49 [89], 2.49 [92]
R (%)	0.40		2.83		0.43	
A (Å^2)	138.72		196.18		106.79	
Φ (eV)	5.89	5.66 [89]	5.49	5.26 [89]	5.64	5.69 [89]
d-band centre (eV)	−2.24		−2.00		−2.44	−2.45 [93]

To understand the possible behaviour and chemical reactivity of the Pt (001), (011) and (111) surfaces, the work function (Φ), was calculated for each pristine surface (Table 1). From our calculations, it can be seen that removing an electron would be easiest from the (001) surface, followed by the (111) and (011) surfaces. Literature showed a similar trend [89] $\Phi_{(011)} < \Phi_{(001)} < \Phi_{(111)}$, with the lowest work function calculated for the (011) surface, followed by the (001) and (111) surfaces. However, the surface area and modelling approximation used have an effect on these values. Likewise will the surface properties and the temperature influence the work function data, which in its isolation cannot be used to predict reactivity.[94]

Previously, it has been shown that adsorption tendencies on transition metal surfaces correlate with the positions of the d-band centre.[95] The overall tendency is that the higher in energy the occupied d-states, the stronger the bond with a molecule that accepts electrons from the metal. From our calculations it was seen that the Pt (111) surface had the highest d-band centre energy, followed by the (001) and (011) surfaces. Literature reported [93] a d-band centre value of -2.45 eV for the Pt (111) surface, which is in excellent agreement with our calculations.

3.2 Adsorption of H_2O and SO_2

To calculate the adsorption behaviour of H_2O on a Pt surface, a single H_2O molecule in a box was modelled, shown in Table 2. The calculated H-O and H-H bond lengths deviated from the experimental gas phase values by less than 0.02 Å and the H-O-H bond angle deviated by only ± 0.07°. Similarly, a single SO_2 molecule in a box was modelled and shown in Table 2. The calculated S-O and O-O bond lengths compared to experimental gas phase values to within ± 0.024 Å and the O-S-O bond angle deviated by only ~1°.

Table 2 – Figure of H_2O and SO_2 with the bond length (Å) and bond angle (°) calculated in this study and compared to experimental and modelled literature values. The colour red is used for oxygen, white for hydrogen and yellow for sulphur.

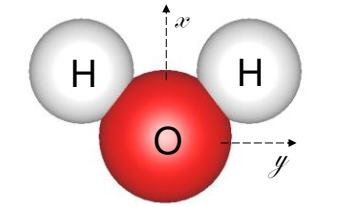

	This Study	Experimental
H-O	0.971	0.958 [96]
H-H	1.535	1.550 [97]
∠H-O-H	104.41	104.48 [96]

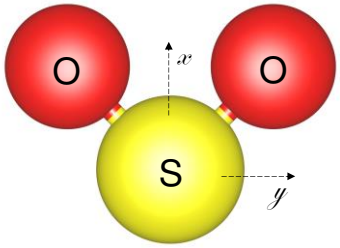

S-O	1.445	1.431 ± 0.002[98]
O-O	2.496	2.460 ± 0.012[98]
∠O-S-O	119.42	118.5 ± 1.0[98]

As shown in Figure 1, various possible adsorption sites for both H_2O and SO_2 were considered on each surface. Adsorbed H_2O molecules on metal surfaces is usually considered to be intact, except when co-adsorbed with other molecules or atoms [99,100]. However, one study investigated a water bilayer on Ru (0001) and suggested that up to half the water molecules are dissociated, with one O-H bond broken in the dissociated water molecules. [101] Similarly, up to 9% of the H_2O molecules dissociated in a study of water bilayers on Pt surfaces [58]. Allowing that it would be less likely to have a single molecule of water

dissociate on the surface, it was still decided to include these data on all three Pt surfaces for reasons of comparison.

Different H_2O adsorption modes [102] were considered on each site, including (i) where all three atoms of the H_2O molecule is parallel to the Pt surface and could interact with the surface, (ii) where the oxygen was bound atop the Pt surface with both H atoms directed away from the surface, (iii) where OH was in the plane of the surface to interact and H was turned upward, and (iv) where one of the H atoms was turned downward to interact with the Pt surface. Five different SO_2 adsorption modes were investigated on each Pt surface, i.e. (i) parallel, (ii) co-planar, (iii) bridging, (iv) O-bonded and (v) S,O-bonded.[103] All five modes were investigated in the various adsorption sites shown in Figure 1. The most favourable adsorption modes will be discussed for each of the Pt (001), (011) and (111) surfaces.

3.2.1 Pt (001)

The most stable and favourable adsorption modes of H_2O and SO_2 on the (001) surface found are shown in Figure 2, with their calculated bond distances and angles of the adsorbed molecules listed in Table 3.

On the (001) surface, four very different H_2O adsorption configurations were observed, i.e. three molecular adsorptions, $Atop_{par}$, $Atop_{4F}$ and $Bridge_{par}$, and one dissociated configuration, $(001)_{diss}$. In the first mode of adsorption, $Atop_{par}$, the H_2O molecule was parallel to the Pt surface with the H-atoms directed toward atop Pt atoms (Figure 2). Here the H-O bond lengths and H-O-H bond angle were similar to the isolated H_2O molecule (Table 2), indicating physisorption to the Pt surface. Similarly, in the second adsorption mode, $Atop_{4F}$, the H_2O molecule was also parallel to the Pt surface with the H-atoms directed toward the 4-fold hollow position, where the O-Pt distance was 2.311 Å and the H2-Pt distances were 2.831 and 2.786 Å for Pt1 and Pt2, respectively. The H-O-H angle correlated with experimental values at 104.48° [104], again suggesting that the water was physisorbed. The third adsorption mode, $Bridge_{par}$, showed the O atom of H_2O bound between two atop Pt atoms, with the H atoms directed toward a 4F hollow. However, the H_2O molecule is not symmetrically parallel to the surface, with a $Pt_{surface}$-O-H1 bond angle of ~8° and a $Pt_{surface}$-O-H2 angle of ~3°. Similar to the other two adsorption modes, we found that the O-H bond lengths and H-O-H bond angle corresponds to the free molecule, indicating physisorption of the H_2O molecule. In the case of $(001)_{diss}$, both the OH and dissociated H atom were bound in the four-fold hollow site, with an O-Pt distance of 2.096 Å and hydroxy H to Pt1 distance of 2.531 Å and 2.956 Å to Pt2. The H-Pt2 distance for the dissociated H was 1.754 Å.

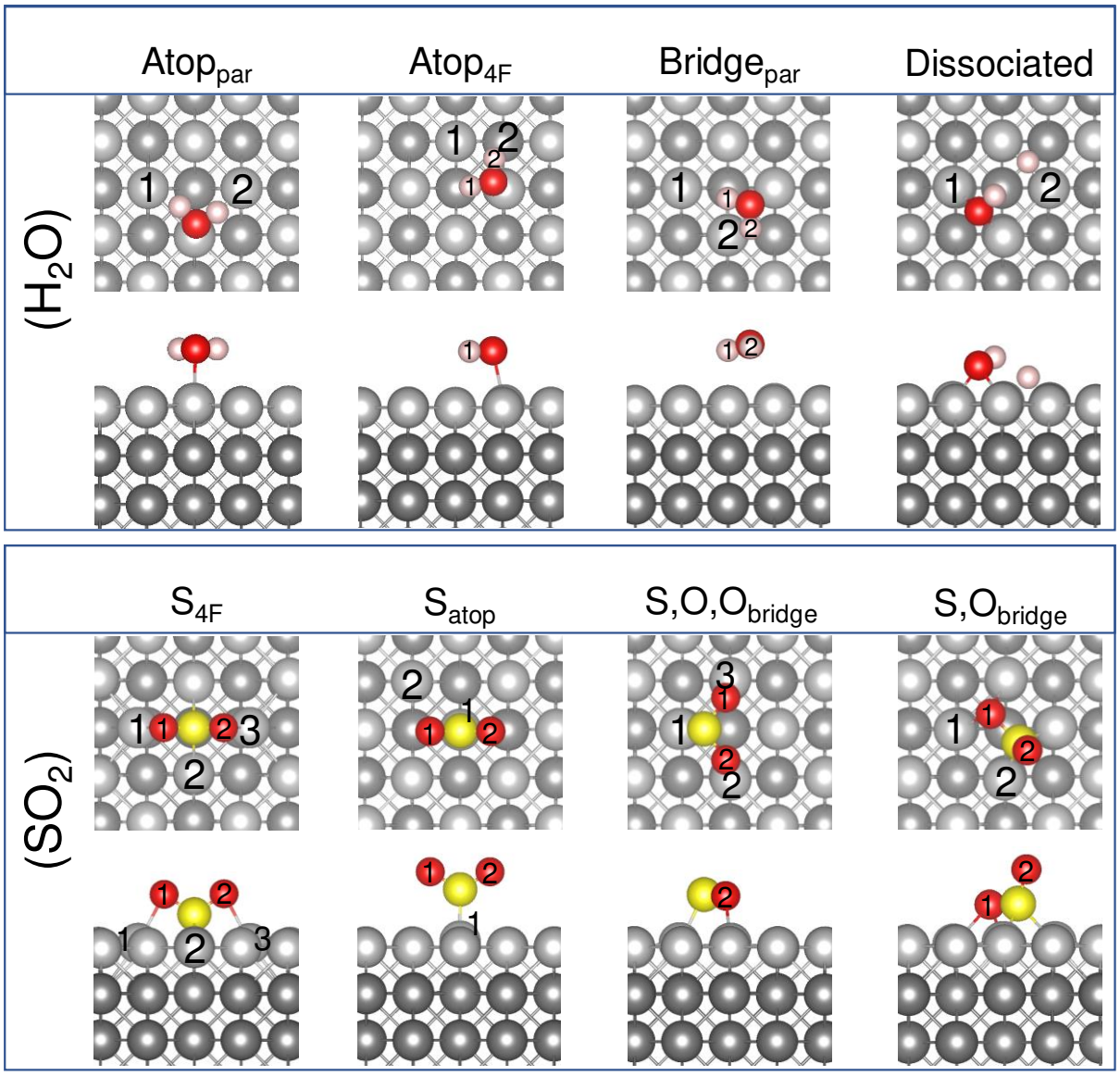

231

232 Figure 2 – Lowest energy adsorption sites of H_2O and SO_2 on the Pt (001) surfaces. The atom colours
233 red denotes oxygen, white for hydrogen and silver for platinum atoms respectively. Again, the lighter
234 silver colour is used to distinguish between the platinum atoms of different layers.
235

Table 3 – Adsorption energy (E_{ads}), charge transfer (Δq), bond distance (d) and angles ($\angle$) of the adsorbed H_2O and SO_2 molecule on the Pt (001) surface.

	H_2O	$Atop_{par}$[68]	$Atop_{4F}$	$Bridge_{par}$	Dissociated[68]
	E_{ads} (eV)	−1.675	−0.510	−1.529	−1.758
	Δq (e)	0.109	0.107	0.052	−0.393
d (Å)	O-Pt	2.311	2.330	2.737	2.096
	H-Pt1	2.831	3.012 (H1), 3.098 (H2)	3.003 (H1)	2.531
	H-Pt2	2.786	4.398 (H2)	2.791 (H1), 2.687 (H2)	2.956, 1.754
	O-H	0.983	0.981	0.981	0.983
∠ (°)	H-O-H	104.55	104.79	104.57	-
	Pt-O-H	97.94	98.67 (H1), 100.0 (H2)	98.49 (H1), 93.39 (H2)	104.55
	SO_2	S_{4F}	S_{atop}	S,O,O_{bridge}	S,O_{bridge}[69]
	E_{ads} (eV)	−1.543	−1.469	−2.085	−2.471
	Δq (e)	−0.392	−0.074	−0.410	−0.349
d (Å)	S-Pt	2.322 (Pt2)	2.155 (Pt1)	2.242 (Pt1)	2.234 (Pt2)
	O-Pt	2.327 (Pt1), 2.358 (Pt3)	3.147 (Pt1), 3.825 (Pt2)	2.126 (O2-Pt2), 2.125 (O1-Pt3)	2.255 (O1-Pt1), 3.082 (O1-Pt2)
	S-O	1.515 (O1), 1.511 (O2)	1.447 (O1), 1.447 (O2)	1.550 (O1), 1.550 (O2)	1.619 (O1), 1.451 (O2)
∠ (°)	O-S-O	111.96	119.00	110.14	110.05
	Pt-S-O	61.03 (Pt1-S-O1)			105.13 (Pt2-S-O1)

The calculated adsorption energies are tabulated in Table 3, which shows that the H_2O molecule is much more strongly bound to surface when it is dissociated, whereas molecular adsorption follows the trend $Atop_{par}$ > $Bridge_{par}$ >> $Atop_{4F}$. In the matter of the dissociated H_2O, we note that a charge of 0.39 e^- was transferred from the Pt surface to the molecule, with the dissociated H atom becoming electron-depleted ($\Delta q = 0.623\ e^-$) relative to the surrounding Pt atoms, whereas the OH part gained electrons ($\Delta q = -1.016\ e^-$). However, in the molecular adsorption on the (001) surface, between 0.5 and 0.11 e^- were donated from the molecule to the surface, and, as also suggested by the positive Δq values, the charge transfer values follow the same trend as the adsorption energies, except in the case of $Atop_{4F}$. From our calculations, it appears that the H_2O molecule would start in the $Atop_{par}$ configuration (−1.675 eV, 0.109 e^-), from where it has to move to the $Atop_{4F}$ configuration (−0.510 eV, 0.107 e^-), with a lower adsorption energy but similar transferred charge, before it dissociates.

During the SO_2 adsorption on the (001) surface, four possible adsorption modes were observed and named according to the adsorption site, i.e. S_{4F}, S_{atop}, S,O,O_{bridge} and S,O_{bridge}. In the first adsorption mode, S_{4F}, the S atom is within a 4F hollow, bound to two surrounding Pt atoms and the two oxygen atoms are bound to the other two surrounding Pt atoms of the same 4F hollow. The S-O bond length is slightly elongated, while the O-S-O bond angle is smaller than for the free SO_2 molecule, which indicates chemisorption on the (001) surface. The second adsorption mode is S_{atop}, where the S atom is bound atop a Pt atom, with the O atoms directed away from the surface. In this case the S-O bond length and O-S-O bond angle correlate with the free SO_2 molecule, because there is limited interaction between the surface and the adsorbed molecule. In the third adsorption mode, i.e. S,O,O_{bridge}, the SO_2 molecule is parallel to the Pt surface, with both O atoms bound to Pt surface atoms. Similar to the S_{4F} configuration, the S-O bonds are elongated, while the O-S-O bond angle is smaller, again indicating chemisorption in this configuration. In the fourth adsorption mode, i.e. S,O_{bridge}, one S-O bond is parallel to the surface, thereby binding to four Pt atoms in a 4F binding site, with the other O atom, O2, directed away from the surface. The S-O2 bond length correlates with the S-O bond length of the free SO_2 molecule, while the S-O1 bond length is elongated due to the attraction to two Pt atoms in the 4F hollow site. In an experimental study of SO_2 adsorption on a Pd (100) surface [38], SO_2 had a S,O_{bridge} geometry with a corresponding S-O and S-Pd bond length of 1.48 and 2.24 Å, respectively. In an SO_2 adsorption study on Ru (001) [105], it was found that the molecular plane of SO_2 was perpendicular to the Ru(001) surface, similar to the S_{atop} and S_{4F} adsorptions here, with a corresponding adsorption energy of 0.538 eV (12.4 kcal/mol). In another study on Cu (100) [30], it was found that at low coverages SO_2 should adsorb preferentially with its molecular plane parallel to the surface, similar to our S,O,O_{bridge} adsorption. However, as the coverage of SO_2 on Cu (100) becomes substantial, the molecule adopts the S,O_{bridge} binding configurations to minimise adsorbate-adsorbate repulsions.

Comparing the adsorption energies of all four SO_2 adsorption modes, we note that the strongest adsorption is observed for the S,O_{bridge} configuration, followed by S,O,O_{brige}, S_{4F} and then S_{atop} modes. In terms of charge transfer, the negative values (Table 3) indicate that electrons were transferred from the Pt surface to the adsorbate. Most charge, i.e. −0.410 e^-, was transferred in the S,O,O_{bridge} adsorption mode, where all three atoms of SO_2 were bound to the Pt surface. The second highest was in S_{4F} (−0.392 e^-), where again the three atoms were bound to the surface, followed by S,O_{bridge} (−0.349 e^-) with only the S-O bond aligned to the surface and, finally, S_{atop} (−0.074 e^-) where only S was bound to the Pt surface.

We note that on this surface, the adsorption sites for both H_2O and SO_2 are similar and they will therefore compete directly for adsorption. In one scenario, if we assume that the Pt surface is first covered with H_2O on all the adsorption sites, the surface should be saturated with electrons from both the surface and the H_2O molecules. If a SO_2 molecule were then to approach this water-covered surface, it should easily displace the H_2O molecules, as the SO_2 can absorb electrons from the surface and has a larger, more favourable adsorption energy, i.e. −2.47 eV for S,O_{bridge} vs −1.68 eV for $Atop_{H2O}$. Looking at the charge density difference in the S,O_{bridge} configuration, we note that the S-O adsorbed onto the Pt surface has a cumulative charge of 0.79 e^- and the O atom directed away from the surface −1.14 e^-. This negatively charged O atom would be available for reactions with either surface-bound molecular H_2O or dissociated $OH^- + H^+$ in the vicinity of the SO_2, which could lead to the formation of HSO_3^-, an intermediary species in the production of hydrogen in the HyS cycle.

3.2.2 Pt (011)

On the (011) surface, five molecularly adsorption modes ($Atop_{par}$, $Atop_{away}$, $Bridge_{H,H}$, $Bridge_{par}$ and $Bridge_{4F}$) and two dissociative modes ($(011)_{diss,A}$ and $(011)_{diss,B}$) were observed for H_2O. In the first adsorption mode, $Atop_{par}$, the H_2O molecule is parallel to the surface, with the O atom bound atop a Pt atom and the H atoms directed towards the (011) channels. The O-H bond lengths and H-O-H bond angle compare to those in the free molecule, which indicates physisorption. In the second adsorption mode, $Atop_{away}$, we found the O atom to be bound between two Pt atoms on the (011) ridge, with the H atoms directed away from the surface. In this adsorption mode, the H-O bond length correlates with the free molecule, although the H-O-H bond angle is larger by ~3°, which could indicate physisorption. In the third adsorption mode ($Bridge_{H,H}$), the H atoms were directed towards the surface, forming a bridge across the (011) channel. Surprisingly, the O-H bond length still correlated with the free molecule, even though the H-O-H bond angle was ~1.5° smaller, which could also indicate physisorption. In the fourth adsorption mode, $Bridge_{par}$, one of the hydrogens of the H_2O molecule points in the direction of the ridge on which it is adsorbed, while the other H points towards the neighbouring ridge, as shown in Figure 3. The O-Pt

distances on the (011) surface are somewhat shorter than on the other surfaces, even though the H-O-H angle differs by less than 1° from the free molecule. In the fifth adsorption mode, $Bridge_{4F}$, one O-H is bound across the (011) channel in the 4F position, while the other H atom is directed away from the surface. As expected, the O-H1 bond length in the channel is slightly elongated, while the O-H2 directed away from the surface is similar to the free molecule. The H-O-H bond angle is larger by ~3°, which again indicates physisorption. Comparing the adsorption energies of the five adsorption modes, it can be seen that the $Bridge_{par}$ configuration will be favoured, followed by $Atop_{par}$, $Bridge_{4F}$, $Atop_{away}$ and only then $Bridge_{H,H}$.

In the dissociated system (Pt $(011)_{diss,A}$), the OH group lies parallel in the valley of Pt atoms and is bound by its oxygen to the Pt atoms on the neighbouring ridges, following the direction of the valley. Similarly, Shi and Sun [106] showed that the dissociated H atom is bound in a bridge position between two Pt atoms on the ridge. In the second dissociated system (Pt $(011)_{diss,B}$), the OH group is again bound to two Pt atoms on neighbouring ridges, following the direction of the valley. However, the dissociated H atom is bound atop a Pt atom on the ridge. The only difference between Pt $(011)_{diss,A}$ and Pt $(011)_{diss,B}$ is the adsorption energy, which is larger by 0.18 eV for the Pt $(011)_{diss,B}$ adsorption, and thus more favoured.

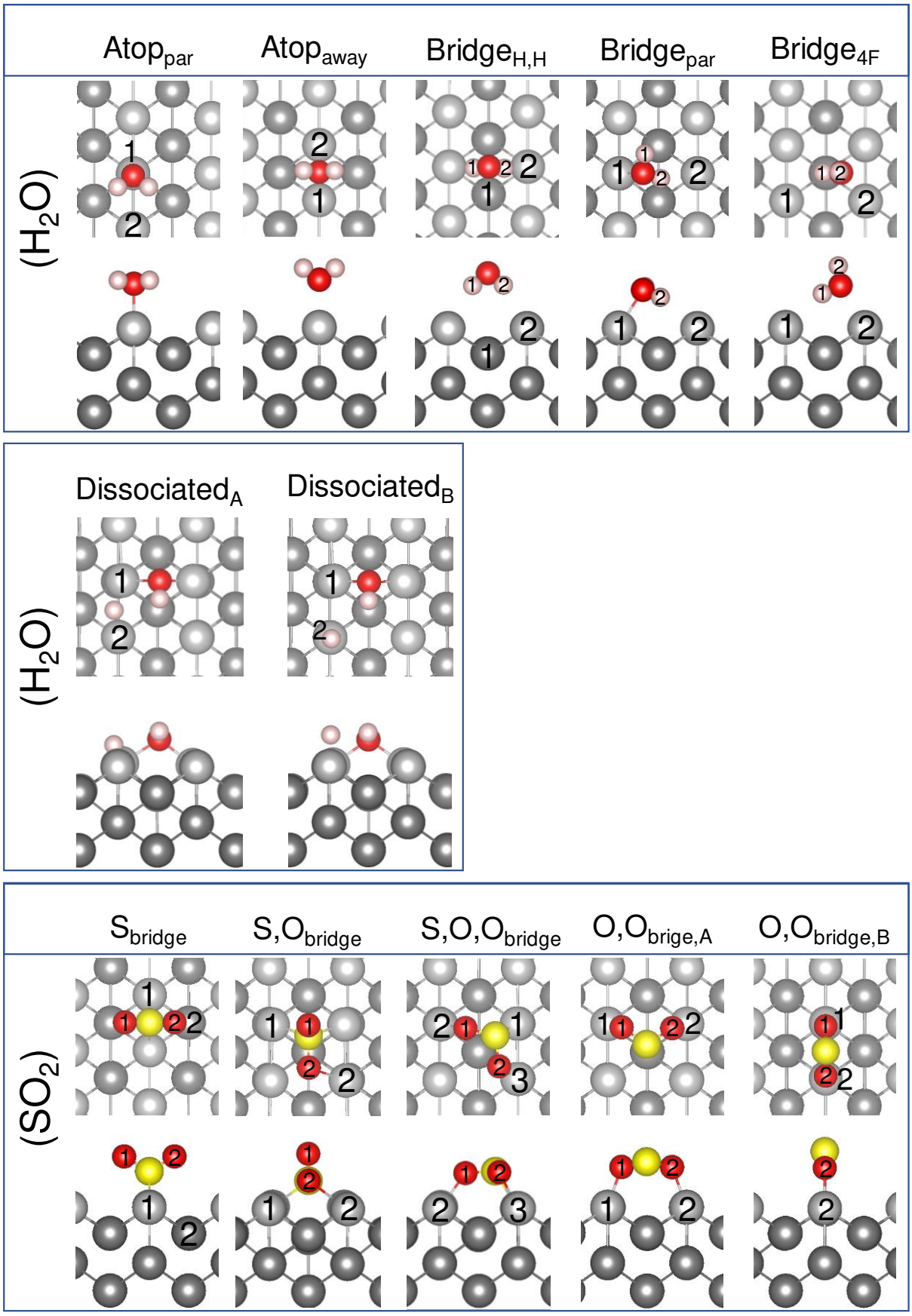

Figure 3 – Lowest energy adsorption sites of H_2O and SO_2 on Pt (011) surface.

Table 4 – Adsorption energy (E_{ads}), charge transfer (Δq), bond distance (d) and angles ($\angle$) of the adsorbed H_2O and SO_2 molecule on the Pt (011) surface.

	H_2O	$Atop_{par}$	$Atop_{away}$	$Bridge_{H,H}$	$Bridge_{par}$[68]	$Bridge_{4F}$	$Diss._{A}$	$Diss._{B}$[68]
	E_{ads} (eV)	−0.543	−0.294	−0.279	−0.699	−0.383	−0.258	−0.434
	Δq (e)	0.098	0.048	−0.044	0.095	0.004	−0.458	−0.472
d (Å)	O-Pt	2.290	2.781 (Pt1)	4.251 (Pt1)	2.240	2.799	2.225	2.162 (Pt1)
			2.745 (Pt2)	3.376 (Pt2)				
	H-Pt1	2.670	3.411	3.724 (H1)	3.050 (H1)	2.836 (H1)	2.619	2.558
				3.746 (H2)				
	H-Pt2	3.298	3.320	2.458 (H2)	2.430 (H2)	3.057 (H1)	3.292 (OH)	1.563
							1.714	
	O-H	0.979	0.974	0.983	0.981 (H1)	0.985 (H1)	0.981	0.982
					1.00 (H2)	0.975 (H2)		
∠ (°)	H-O-H	105.25	107.11	102.91	103.76	107.28	-	-
	Pt-O-H	101.90 (Pt1)	122.93 (Pt1)	51.78 (Pt1-O-H1)	101.86 (H1)	95.65 (Pt2-O-H1)	102.51	102.28 (Pt1)
			118.32 (Pt2)	53.19 (Pt1-O-H2)	99.40 (H2)	143.73 (Pt2-O-H2)		

	SO_2	S_{bridge}[69]	S,O_{bridge}	S,O,O_{bridge}[69]	$O,O_{bridge,A}$	$O,O_{bridge,B}$
	E_{ads} (eV)	−2.282	−2.188	−2.390	−1.327	−1.171
	Δq (e)	−0.198	−0.454	−0.432	−0.393	−0.340
d (Å)	S-Pt	2.263 (Pt1)	2.290 (Pt1)	2.243 (Pt1)	3.147 (Pt1)	3.253 (Pt1)
	O-Pt	3.144 (O1-Pt1)	3.213 (O1-Pt1)	2.114 (O1-Pt2)	2.122 (O1-Pt1)	2.095 (O1-Pt1)
	S-O	3.934 (O2-Pt2)	2.380 (O2-Pt2)	2.120 (O2-Pt3)	2.125 (O2-Pt2)	2.094 (O2-Pt2)
	O-S-O	1.458 (O1)	1.458 (O1)	1.543 (O1)	1.527 (O1)	1.518 (O1)
∠ (°)	Pt-S-O	1.458 (O2)	1.590 (O2)	1.563 (O2)	1.526 (O2)	1.518 (O2)
	E_{ads} (eV)	118.88	111.01	111.01	110.82	112.97

The relative adsorption energies for the water molecule are smaller than observed on the (001) surface and they follow the trend of $Bridge_{par}$ > $Atop_{par}$ > $Bridge_{4F}$ > $Atop_{away}$ > $Bridge_{H,H}$. However, the adsorption energies of the dissociated water are small and similar to some of the molecularly adsorbed H_2O configurations, indicating that there is little incentive for dissociation to occur on the (011) surface. From the charge transfer calculations it can be seen, that, similar to the (001) surface, in molecularly adsorbed H_2O, electrons are transferred from the molecule to the Pt surface, which is highest (~ 0.1 e^-) for the most favoured configurations $Bridge_{par}$ and $Atop_{par}$. However, it is interesting that the $Bridge_{H,H}$ configuration adsorbs electrons (−0.044 e^-) from the Pt surface. With the H atoms directed toward the Pt surface and electrons being donated into the molecule, dissociation could occur, possibly leading to the H_2O_{diss} configurations, although the energetic incentive is low. In the dissociated H_2O, charge transfer of between 0.4 and 0.5 e^- occurs from the Pt surfaces to the molecule. As expected, the dissociated H atom is electron-depleted (Δq = 1.000 e^-) and OH gained nearly an extra 50% electron density (Δq = −1.458 e^-), owing to the adsorption manner of the dissociated H and OH, which are pulled into the (011) framework, thereby favouring electron transfer to and from the Pt surface.

In the adsorption of SO_2 on the (011) surface, five possible adsorption modes were observed, i.e. S_{bridge}, S,O_{bridge}, S,O,O_{bridge}, $O,O_{bridge,A}$ and $O,O_{bridge,B}$. In the first adsorption mode, i.e. S_{bridge}, the SO_2 molecule had the same geometry to the S_{atop} configuration on the (001) surface, with the S bound to the Pt surface and the two O atoms directed away from the surface, although here the S atom is located between two ridge Pt atoms. The S-O bond length and O-S-O bond angle was similar to the free SO_2 molecule, due to limited interaction between the surface and adsorbate. In the second adsorption mode, i.e. S,O_{bridge}, the S-O bond is parallel to the channel on the (011) surface, with the other O atom directed away from the surface. The S atom is bound across the ridge to two Pt atoms and the O atom to another two Pt atoms of a 4F hollow site. The S-O bond lengths and O-S-O bond angle follow the same trend as for the S,O_{bridge} adsorption mode on the (001) surface where the free S-O bond length is shorter than the bound S-O bond length and the O-S-O bond angle smaller than 119°, indicating physisorption. In the third adsorption mode, i.e. S,O,O_{bridge}, the SO_2 molecule is parallel to the Pt surface with two O atoms bound to two Pt atoms on the (011) ridge, forming an O-O-bridge with Pt diagonally across the (011) channel. Due to the formation of this Pt-O bond, the S-O bond is slightly elongated, while the O-S-O bond angle is smaller than in the free molecule. Similarly, in the fourth adsorption mode, i.e. $O,O_{bridge,A}$, the SO_2 molecule lies parallel to the surface, forming an O-O-bridge with Pt directly across the (011) channel. Again, the S-O bond length is elongated, while the O-S-O bond angle is smaller. In the fifth adsorption mode, $O,O_{bridge,B}$ the molecules also form an O-O-bridge, but with two Pt atoms on the same (011) ridge, with the S atom directed away from the surface. As in the other adsorption modes, the S-O bond lengths are elongated, while the O-S-O bond angle is smaller than in the free molecule.

When we compare the SO_2 adsorption energies, it is evident that the most likely adsorption to occur is the S,O,O_{bridge} configuration, followed by S_{bridge} > S,O_{bridge} > $O,O_{bridge,A}$ > $O,O_{bridge,B}$. It has been shown in the literature [107] for SO_2 adsorbed onto Ag (110), that the S_{bridge} adsorption mode dominates, whereas on the Ni (110) surface, both S,O,O_{bridge} and $O,O_{brigde,A}$ adsorptions occur.

In terms of charge transfer in the adsorbed SO_2 molecules, the trend on the (011) surface is similar to the (001) surface, with Δq the highest where all three atoms (S, O1 and O2) are adsorbed onto the Pt surface, followed by the adsorption of two atoms (S and O or O1 and O2) and then one atom (S). However, on this surface, e.g. in S,O_{bridge} with two adsorbed atoms (S and O2) bound between four Pt atoms, more charge is transferred to SO_2, i.e. −0.454 e^-, followed by S,O,O_{bridge} (−0.432 e^-) with three atoms bound to the surface, next $O,O_{bridge,A}$ (−0.393 e^-) with only O-O on the surface, then $O,O_{bridge,B}$ (−0.340 e^-) also with O-O on the surface and, finally, S_{bridge} (−0.198 e^-) where only S was bound to the Pt surface.

Comparing the adsorption of H_2O and SO_2, in terms of the most favourable adsorption energies, we note that the $Brigde_{par}$ (H_2O configuration) and the S,O,O_{bridge} configuration directly compete for adsorption sites. However, in these specific configurations, the H from H_2O and the O from SO_2 can be directed towards each other for a reaction to occur. A similar result is seen in the second most favourable positions, i.e. $Atop_{par}$ (H_2O configuration) and S_{bridge} configuration, where their specific binding geometries would allow reaction between H_2O and SO_2 to occur. If we again assume that the Pt surface is first covered with H_2O on all the adsorption sites, an approaching SO_2 molecule should be able to displace the H_2O as the SO_2 then absorbs electrons from the surface. The charge density distributions in the S,O,O_{bridge} and S_{bridge} configurations are similar to the (001) surface, with a cumulative charge of 0.63 e^- and 0.98e^-, respectively, but −1.07 e^- and −1.18 e^-, respectively, in the O atom directed away from the surface. This negatively charged O atom would be available for reactions with either the molecular H_2O or dissociated OH + H in the vicinity as a first step in the HyS process.

3.3.3 Pt (111)

On the (111) surface only one molecular ($Atop_{par}$) and one dissociative ($(111)_{diss}$) adsorption mode for H_2O were observed. In the $Atop_{par}$ adsorption, the H_2O molecule adsorbs parallel to the Pt surface, with one H atom directed towards a surface Pt (Pt1) and the other in the direction of a *fcc* Pt (Pt2) (Figure 4). Similarly, Carrasco and co-workers [108] showed that the most stable single H_2O molecule adsorption was atop the Pt atom and parallel to the surface. In this work, the H-O-H angle correlated with literature at 104.94 and the calculated O-Pt distance was 2.386 Å, however literature reported the O-Pt distance between 2.49 and 2.82 Å,[108] suggesting that water may bind more strongly to the Pt (111) surface than previously indicated.[108] Similar to the $(001)_{diss}$ and $(011)_{diss}$ systems, on the (111) surface the O from

the dissociated OH group were bound in a bridge position between two surface Pt atoms. The dissociated hydrogen was in a neighbouring *fcc* hollow site, which was also reported [106] as energetically the most stable adsorption mode for hydrogen on the Pt (111) surface.

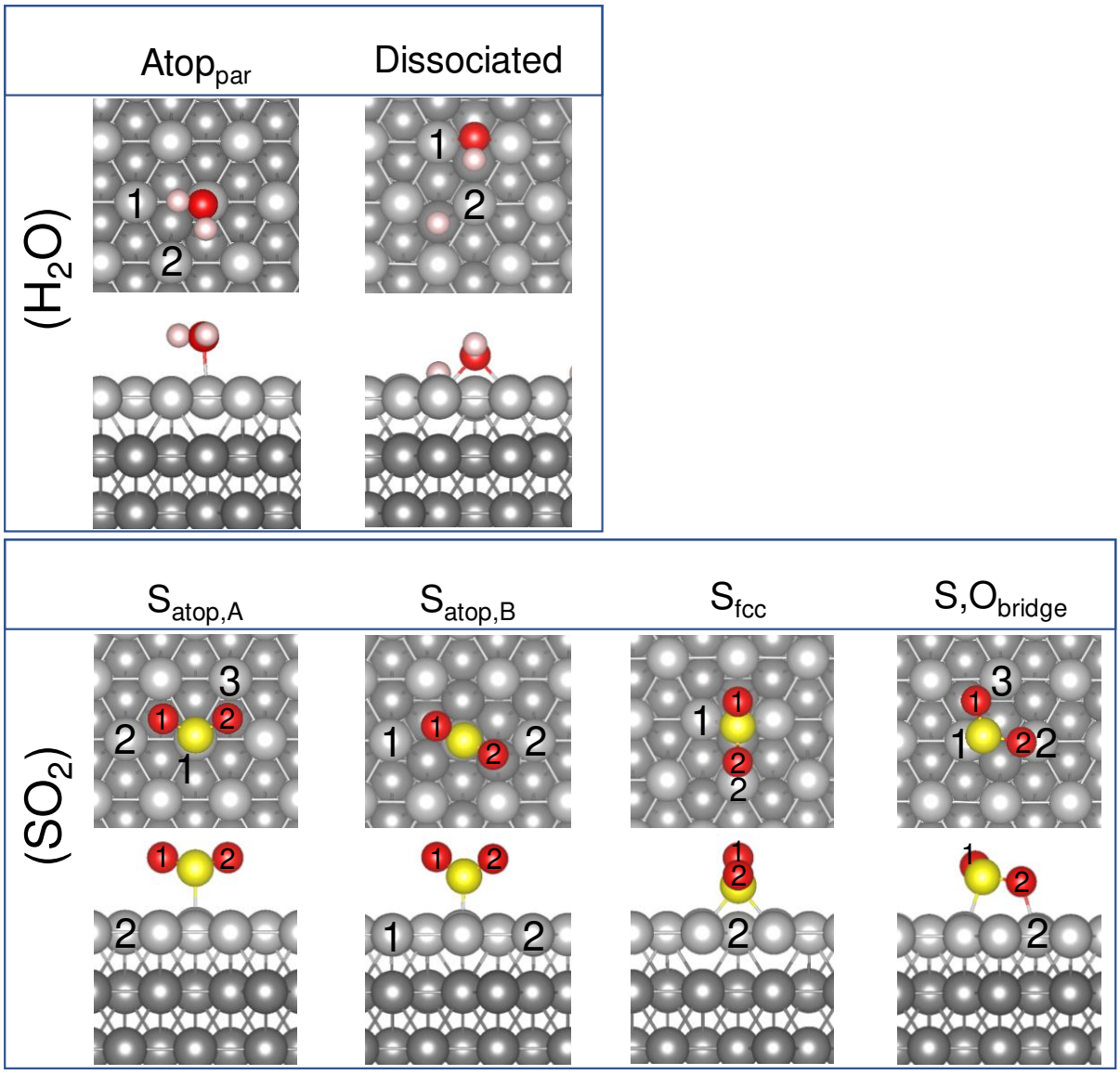

Figure 4 – Lowest energy adsorption sites of H_2O and SO_2 on the Pt (111) surface.

Table 5 – Adsorption energy (E_{ads}), charge transfer (Δq), bond distance (d) and angles ($\angle$) of the adsorbed H_2O and SO_2 molecule on the Pt (111) surface.

	H_2O	$Atop_{par}$[68]		Dissociated[68]		Literature
	E_{ads} (eV)	−0.464		−0.380		-0.35**[109]
	Δq (e)	0.087		−0.338		
d (Å)	O-Pt	2.386		2.169		2.36**[109]
	H-Pt1	2.973		2.591		
	H-Pt2	3.164		3.317 (H1), 1.873 (H2)		
	O-H	0.981		0.983		0.98**[109]
∠ (°)	H-O-H	104.94		-		104.48*[104], 106**[109]
	Pt-O-H	97.72		104.14		97**[109]
	SO_2	$S_{atop,A}$	$S_{atop,B}$	S_{fcc}[69]	S,O_{bridge}	Literature
	E_{ads} (eV)	−1.598	−1.242	−1.852	−0.524	-1.099*[110], -1.218*[24]
	Δq (e)	−0.452	−0.106	−0.240	−0.370	
d (Å)	S-Pt	2.354 (Pt1)	2.178	2.273 (Pt1)	2.326	2.31*[24]
	O-Pt	3.326 (O1-Pt2)	3.631 (O1-Pt1)	3.254 (O1-Pt1)	3.069 (O1-Pt3)	2.30*[24]
		3.267 (O2-Pt3)	3.483 (O2-Pt2)	2.419 (O2-Pt2)	2.148 (O2-Pt2)	
	S-O	1.467 (O1)	1.446 (O1)	1.450 (O1)	1.476 (O1)	1.47 (O1)*[24]
		1.468 (O2)	1.446 (O2)	1.500 (O2)	1.552 (O2)	1.54 (O2)*[24]
∠ (°)	O-S-O	117.64	119.42	115.27	112.43	155.5*[24]
	Pt-S-O	107.79 (Pt-S-O1)	120.05 (Pt-S-O1)	120.21 (Pt1-S-O1)	107.04 (Pt1-S-O1)	
		107.52 (Pt-S-O2)	120.53 (Pt-S-O2)	108.84 (Pt1-S-O2)	99.16 (Pt1-S-O2)	

The calculated adsorption energies (Table 5) show that the water molecule does not bind as strongly to the (111) surface as on the (001) and to a lesser extent (011) surfaces, indicating that adsorption and dissociation is favoured on the (001) surface. Literature showed that adsorption energies were dependant on the type of dispersion correction functional used [108], and reported monomer adsorption energies specifically for the Pt (111) surface between −0.24 and −0.40 eV. These values are in fair agreement with our adsorption energy calculated for the (111) surface, but again indicating somewhat stronger binding in this study compared to the literature [108]. Comparing our adsorption energies to that of the dissociated water on all the surfaces, we note that generally adsorption is energetically preferred on the (001) surface, both for the molecular and dissociated H_2O adsorptions, followed by the (111) and (011) surfaces. On thermodynamic grounds, dissociation should not occur on the (111) surface, where the binding of the dissociated molecule is energetically less favourable than molecular adsorption.

With the adsorption of SO_2 on the (111) surface, four possible adsorption modes were observed, i.e. $S_{atop,A}$, $S_{atop,B}$, S_{fcc} and S,O_{bridge}. In $S_{atop,A}$ the S atom is bound atop a Pt atom with the O atoms directed ($Pt_{surface}$-S-O angle ~18°) away from the surface. The geometry of the bound SO_2 is similar to the free SO_2 molecule, indicating physisorption of the molecule. Similarly, in $S_{atop,B}$, the S is bound atop a Pt atom with the O atoms directed away from the Pt atoms, with a $Pt_{surface}$-S-O bond angle of 30°. This configuration is similar to the S_{atop} adsorption mode on the Pt (001) surface, with S-O bond length and O-S-O bond angle corresponding to the free SO_2 molecule, again indicating physisorption of the molecule. In the third adsorption mode, S_{fcc}, one S-O bond lies in the plane of the surface and the second O atom is directed away from the surface on the *fcc* binding site. As seen before, the parallel S-O bond is elongated, and the O-S-O angle has decreased due to the binding mode. S,O_{bridge} resembles a configuration between $S_{atop,A}$ and S_{fcc}, where one S-O bond is bound to two atop Pt atoms, with a $Pt_{surface}$-S-O2 angle of ~9°, while the other S-O bond is pointed slightly away from the surface with a $Pt_{surface}$-S-O1 angle of ~17°. The S-O2 bond length is slightly elongated due to the bond with the atop Pt atoms. Lin and co-workers [24] identified similar adsorption modes, of which the most likely were S_{fcc}, $S_{atop,B}$ and S,O_{bridge} with adsorption energies ranging between 0.93 and 1.01 eV. When we compare the different adsorption energies, we find that S_{fcc} has the largest adsorption energy and is therefore the most likely configuration to occur, followed by $S_{atop,B} > S_{atop,B} > S,O_{bridge}$.

In terms of charge transfer (Table 5) between SO_2 and Pt (111), the trend is similar to the (001) and (011) surfaces, with a maximum Δq when all three atoms (S, O1 and O2) are adsorbed onto the Pt surface, although $S_{atop,A}$ with only S adsorbed is an outlier, as this configuration leads to the largest charge transfer (Δq = −0.452 e^-). However, the other adsorption modes follow the trend, i.e. three adsorbed atoms (S, O1 and O2) are bound in S,O_{bridge} (−0.370 e^-), followed by two adsorbed atoms (S and O2) in S_{fcc} (−0.240 e^-) and finally $S_{atop,B}$ (−0.106 e^-) where only S was bound to the Pt surface.

The calculated modes and energies of adsorption of SO_2 on the (111) are in fair agreement with the work by Lin and co-workers [24] who calculated adsorption energies for the Pt (111) surface ranging between 0.93 and 1.01 eV, depending on adsorption mode and the dispersion correction functional chosen.

If we compare the adsorption sites of both H_2O and SO_2 on the (111) surface, we note that there is no direct competition for the most favourable adsorption configurations, $Atop_{par}$ and S_{fcc}, but there is for the second most favourable configuration, $S_{atop,A}$. A comparison of the adsorption energies of H_2O and SO_2 shows a difference of between 1.1 and 1.4 eV, indicating that if a SO_2 molecule were to approach a water-covered surface, the H_2O could be displaced, as the SO_2 absorbs electrons from the surface and has a more favourable adsorption energy. Looking at the charge density difference in the S_{fcc} configuration, we note that the S-O adsorbed onto the Pt surface has a cumulative charge of 0.91 e^- with −1.15 e^- in the O atom directed away from the surface. However, in the $S_{atop,A}$ configuration, the charge is distributed equally through the molecule, with a charge transfer of 3.00 e^- and −1.72 e^- for S and each O atom, respectively. These O atoms may be available for reactions with the H_2O molecules.

4. Conclusions

In this study, we have employed density functional theory calculations to predict the behaviour of H_2O and SO_2 with the Pt (001), (011), and (111) surfaces. Our results show that a H_2O molecule will preferentially adsorb dissociatively on the (001) surface, but on both the (011) and (111) surfaces, the H_2O molecule adsorbs parallel atop the Pt surface atoms. Charge transfer analysis shows that the molecularly bound H_2O provides ~0.1 e^- to the Pt surface, whereas in the dissociated case ~0.4 e^- transferred from the surface to the molecule.

When SO_2 adsorbs onto Pt, was observed that on both the (001) and (111) surfaces, S-O will preferentially adsorb onto the surface with one O atom directed away from the surface. However, on the (011) surface, SO_2 lies parallel to the surface with one S-O pair bound across the channel and the other S-O pair bound on the ridge between two Pt atoms. SO_2 can act as both a σ-donor or π-acceptor[111], and when the π-acceptor aspect dominates, π bonds are formed between the SO_2 and the metal, causing the molecule to adsorb in a parallel orientation on the surface, as seen on the (011) surface. In contrast, when σ-bonding dominates, the molecule adsorbs perpendicular to the surface planes, as shown to occur on the (001) and (111) surfaces. Charge transfer analysis shows that during adsorption, between 0.24 and 0.43 e^- is transferred from the surface to the molecule.

Taking into account all the adsorption energy and charge transfer data of both H_2O and SO_2 on all three Pt surfaces, it can be concluded that generally both molecules compete for the same adsorption sites,

where the strong binding of SO_2 to the surface sites should enable it to compete effectively to adsorb onto the Pt surfaces at the expense of water adsorption.

Future work will include the consideration of an explicit mixture of H_2O and SO_2 on the various Pt surfaces, as well as the SO_2 oxidation mechanism catalysed by the Pt metal.

5. Acknowledgements

We acknowledge the Economic and Social Research Council (ESRC grant No. ES/N013867/1) and the National Research Foundation, South Africa, for a Newton Fund PhD student exchange grant, and the Engineering and Physical Sciences Research Council (EPSRC grants No. EP/K016288/1 and EP/K009567/2) for research funding. This work was performed using the computational facilities of the Advanced Research Computing @ Cardiff (ARCCA) Division; Cardiff University; and the Centre of High-Performance Computing (CHPC) in Cape Town, South Africa. In addition, the calculations were carried out using the Supercomputing Facilities at Cardiff University operated by ARCCA on behalf of the HPC Wales and Supercomputing Wales (SCW) projects. We acknowledge the support of the latter, which is part-funded by the European Regional Development Fund (ERDF) via Welsh Government. We wish to acknowledge the use of the EPSRC-funded National Chemical Database Service hosted by the Royal Society of Chemistry. D.S.-C. is grateful to the Department of Science and Technology (DST) and the National Research Foundation (NRF) of South Africa for the provision of a Postdoctoral Fellowship for Early Career Researchers from the United Kingdom. M.J.U. would like to acknowledge the National Research Foundation (NRF – Grant number 116728) for their financial support and the North-West University for their support and resources. All data created during this research are openly available from Cardiff University's Research Portal at http://dx.doi.org/10.17035/d.2020.0102392217.

6. References

1. Igliński, H.; Babiak, M. Analysis of the Potential of Autonomous Vehicles in Reducing the Emissions of Greenhouse Gases in Road Transport. *Procedia Eng.* **2017**, *192*, 353–358, doi:10.1016/j.proeng.2017.06.061.

2. EASA *European Aviation Environmental Report 2016*; 2019; Vol. 40;.

3. Rt Hon Michael Gove *Clean Air Strategy Plan*; 2019;

4. Junginger, M.; Hittinger, E.; Williams, E.; Wiser, R. Onshore wind energy. In *Technological Learning in the Transition to a Low-Carbon Energy System*; Elsevier, 2020; pp. 87–102.

5. Varela-Vázquez, P.; Sánchez-Carreira, M. del C.; Rodil-Marzábal, Ó. A novel systemic approach for analysing offshore wind energy implementation. *J. Clean. Prod.* **2019**, *212*, 1310–1318, doi:10.1016/j.jclepro.2018.12.079.

6. Sarver, T.; Al-Qaraghuli, A.; Kazmerski, L.L. A comprehensive review of the impact of dust on the use of solar energy: History, investigations, results, literature, and mitigation approaches. *Renew. Sustain. Energy Rev.* **2013**, *22*, 698–733, doi:10.1016/j.rser.2012.12.065.

7. Gong, J.; Li, C.; Wasielewski, M.R. Advances in solar energy conversion. *Chem. Soc. Rev.* **2019**, *48*, 1862–1864, doi:10.1039/C9CS90020A.

8. Carrillo, A.J.; González-Aguilar, J.; Romero, M.; Coronado, J.M. Solar Energy on Demand: A Review on High Temperature Thermochemical Heat Storage Systems and Materials. *Chem. Rev.* **2019**, *119*, 4777–4816, doi:10.1021/acs.chemrev.8b00315.

9. Falchetta, G.; Gernaat, D.E.H.J.; Hunt, J.; Sterl, S. Hydropower dependency and climate change in sub-Saharan Africa: A nexus framework and evidence-based review. *J. Clean. Prod.* **2019**, *231*, 1399–1417, doi:10.1016/j.jclepro.2019.05.263.

10. Sharma, S.; Waldman, J.; Afshari, S.; Fekete, B. Status, trends and significance of American hydropower in the changing energy landscape. *Renew. Sustain. Energy Rev.* **2019**, *101*, 112–122, doi:10.1016/j.rser.2018.10.028.

11. Jurasz, J.; Canales, F.A.; Kies, A.; Guezgouz, M.; Beluco, A. A review on the complementarity of renewable energy sources: Concept, metrics, application and future research directions. *Sol. Energy* **2020**, *195*, 703–724, doi:10.1016/j.solener.2019.11.087.

12. Edwin, M.; Nair, M.S.; Joseph Sekhar, S. A comprehensive review for power production and economic feasibility on hybrid energy systems for remote communities. *Int. J. Ambient Energy* **2020**, 1–13, doi:10.1080/01430750.2020.1712252.

13. van der Roest, E.; Snip, L.; Fens, T.; van Wijk, A. Introducing Power-to-H3: Combining renewable electricity with heat, water and hydrogen production and storage in a neighbourhood. *Appl. Energy* **2020**, *257*, 114024, doi:10.1016/j.apenergy.2019.114024.

14. de Bruijn, F. The current status of fuel cell technology for mobile and stationary applications. *Green Chem.* **2005**, *7*, 132–150, doi:10.1039/b415317k.

15. Nikolaidis, P.; Poullikkas, A. A comparative overview of hydrogen production processes. *Renew. Sustain. Energy Rev.* **2017**, *67*, 597–611, doi:10.1016/j.rser.2016.09.044.

16. Singh, V.; Das, D. Chapter 3 - Potential of Hydrogen Production From Biomass. In *Science and*

Engineering of Hydrogen-Based Energy Technologies; Miranda, P.E.V. de, Ed.; Academic Press, 2018; pp. 123–164 ISBN 978-0-12-814251-6.

17. Revankar, S.T. Chapter 4 - Nuclear Hydrogen Production. In *Storage and Hybridization of Nuclear Energy*; Bindra;, H., Revankar, S., Eds.; Academic Press, 2019; pp. 49–117 ISBN 978-0-12-813975-2.

18. Ahammad, S.Z.; Sreekrishnan, T.R. Energy from Wastewater Treatment. In *Bioremediation and Bioeconomy*; Elsevier, 2016; pp. 523–536.

19. Xue, L.; Zhang, P.; Chen, S.; Wang, L. Pt-based bimetallic catalysts for SO2-depolarized electrolysis reaction in the hybrid sulfur process. *Int. J. Hydrogen Energy* **2014**, *39*, 14196–14203, doi:10.1016/j.ijhydene.2014.02.128.

20. O'Brien, J.A.; Hinkley, J.T.; Donne, S.W.; Lindquist, S.E. The electrochemical oxidation of aqueous sulfur dioxide: A critical review of work with respect to the hybrid sulfur cycle. *Electrochim. Acta* **2010**, *55*, 573–591, doi:10.1016/j.electacta.2009.09.067.

21. Appleby, A.J.; Pinchon, B. Electrochemical aspects of the H2SO4SO2 thermoelectrochemical cycle for hydrogen production. *Int. J. Hydrogen Energy* **1980**, *5*, 253–267, doi:10.1016/0360-3199(80)90070-1.

22. Lu, P.W.T.; Ammon, R.L. An Investigation of Electrode Materials for the Anodic Oxidation of Sulfur Dioxide in Concentrated Sulfuric Acid. *J. Electrochem. Soc.* **1980**, *127*, 2610, doi:10.1149/1.2129530.

23. Colón-Mercado, H.R.; Hobbs, D.T. Catalyst evaluation for a sulfur dioxide-depolarized electrolyzer. *Electrochem. commun.* **2007**, *9*, 2649–2653, doi:10.1016/j.elecom.2007.08.015.

24. Lin, X.; Hass, K.C.; Schneider, W.F.; Trout, B.L. Chemistry of Sulfur Oxides on Transition Metals I: Configurations, Energetics, Orbital Analyses, and Surface Coverage Effects of SO 2 on Pt(111). *J. Phys. Chem. B* **2002**, *106*, 12575–12583, doi:10.1021/jp026128f.

25. Somorjai, G.A. On the mechanism of sulfur poisoning of platinum catalysts. *J. Catal.* **1972**, *27*, 453–456, doi:10.1016/0021-9517(72)90183-2.

26. Nasri, N.S.; Jones, J.M.; Dupont, V.A.; Williams, A. A Comparative Study of Sulfur Poisoning and Regeneration of Precious-Metal Catalysts. *Energy & Fuels* **1998**, *12*, 1130–1134, doi:10.1021/ef980104j.

27. Polcik, M.; Wilde, L.; Haase, J.; Brena, B.; Cocco, D.; Comelli, G.; Paolucci, G. Adsorption and temperature-dependent decomposition of SO2 on Cu(100) and Cu(111): A fast and high-resolution

core-level spectroscopy study. *Phys. Rev. B* **1996**, *53*, 13720–13724, doi:10.1103/PhysRevB.53.13720.

28. Polčik, M.; Wilde, L.; Haase, J. SO2-induced surface reconstruction of Cu(111): An x-ray-absorption fine-structure study. *Phys. Rev. B* **1998**, *57*, 1868–1874, doi:10.1103/PhysRevB.57.1868.

29. Wilburn, M.S.; Epling, W.S. SO2 adsorption and desorption characteristics of Pd and Pt catalysts: Precious metal crystallite size dependence. *Appl. Catal. A Gen.* **2017**, *534*, 85–93, doi:10.1016/j.apcata.2017.01.015.

30. Rodriguez, J.A.; Ricart, J.M.; Clotet, A.; Illas, F. Density functional studies on the adsorption and decomposition of SO2 on Cu(100). *J. Chem. Phys.* **2001**, *115*, 454–465, doi:10.1063/1.1377884.

31. Yokoyama, T.; Terada, S.; Yagi, S.; Imanishi, A.; Takenaka, S.; Kitajima, Y.; Ohta, T. Surface structures and electronic properties of SO2 adsorbed on Ni(111) and Ni(100) studied by S K-edge X-ray absorption fine structure spectroscopy. *Surf. Sci.* **1995**, *324*, 25–34, doi:10.1016/0039-6028(94)00692-X.

32. Terada, S.; Imanishi, A.; Yokoyama, T.; Takenaka, S.; Kitajima, Y.; Ohta, T. Surface structure of SO2 adsorbed on Ni(110) studied by S K-edge X-ray absorption fine structure spectroscopy. *Surf. Sci.* **1995**, *336*, 55–62, doi:10.1016/0039-6028(95)00514-5.

33. Zebisch, P.; Weinelt, M.; Steinrück, H.-P. Sulphur dioxide adsorption on the Ni(110) surface. *Surf. Sci.* **1993**, *295*, 295–305, doi:10.1016/0039-6028(93)90276-P.

34. Ahner, J.; Effendy, A.; Vajen, K.; Wassmuth, H.-W. Chemisorption and multilayer adsorption of SO2 on Ag(111) and Ag(110). *Vacuum* **1990**, *41*, 98–101, doi:10.1016/0042-207X(90)90285-7.

35. Solomon, J.L.; Madix, R.J.; Wurth, W.; Stohr, J. NEXAFS and EELS study of the orientation of sulfur dioxide on silver(110). *J. Phys. Chem.* **1991**, *95*, 3687–3691, doi:10.1021/j100162a046.

36. Ku, R.C.; Wynblatt, P. SO2 adsorption on Rh(110) and Pt(110) surfaces. *Appl. Surf. Sci.* **1981**, *8*, 250–259, doi:10.1016/0378-5963(81)90120-3.

37. Rodriguez, J.A.; Jirsak, T.; Chaturvedi, S. Reaction of S2 and SO2 with Pd/Rh(111) surfaces: Effects of metal–metal bonding on sulfur poisoning. *J. Chem. Phys.* **1999**, *110*, 3138–3147, doi:10.1063/1.477910.

38. Terada, S.; Sakano, M.; Kitajima, Y.; Yokoyama, T.; Ohta, T. Adsorption of SO2 on Pd(100) Studied by S K-Edge XAFS. *Le J. Phys. IV* **1997**, *7*, C2-703-C2-704, doi:10.1051/jp4:1997211.

39. Burke, M.L.; Madix, R.J. Hydrogen on Pd(100)-S: the effect of sulfur on precursor mediated

adsorption and desorption. *Surf. Sci.* **1990**, *237*, 1–19, doi:10.1016/0039-6028(90)90515-A.

40. Saleh, J.M. Interaction of sulphur compounds with palladium. *Trans. Faraday Soc.* **1970**, *66*, 242, doi:10.1039/tf9706600242.

41. Burke, M.L.; Madix, R.J. SO2 structure and reactivity on clean and sulfur modified Pd(100). *Surf. Sci.* **1988**, *194*, 223–244, doi:10.1016/0039-6028(94)91257-2.

42. Astegger, S.; Bechtold, E. Adsorption of sulfur dioxide and the interaction of coadsorbed oxygen and sulfur on Pt(111). *Surf. Sci.* **1982**, *122*, 491–504, doi:10.1016/0039-6028(82)90098-X.

43. Köhler, U.; Wassmuth, H.-W. SO2 adsorption and desorption kinetics on Pt(111). *Surf. Sci.* **1983**, *126*, 448–454, doi:10.1016/0039-6028(83)90742-2.

44. Sun, Y.-M.; Sloan, D.; Alberas, D.J.; Kovar, M.; Sun, Z.-J.; White, J.M. SO2 adsorption on Pt(111): HREELS, XPS and UPS study. *Surf. Sci.* **1994**, *319*, 34–44, doi:10.1016/0039-6028(94)90567-3.

45. Polčik, M.; Wilde, L.; Haase, J.; Brena, B.; Comelli, G.; Paolucci, G. High-resolution XPS and NEXAFS study of SO2 adsorption on Pt(111): two surface SO2 species. *Surf. Sci.* **1997**, *381*, L568–L572, doi:10.1016/S0039-6028(97)00060-5.

46. Lin, X.; Schneider, W.F.; Trout, B.L. Chemistry of sulfur oxides on transition metals. II. Thermodynamics of sulfur oxides on platinum(111). *J. Phys. Chem. B* **2004**, *108*, 250–264, doi:10.1021/jp035306h.

47. Chen, C.-H.; Halford, A.; Walker, M.; Brennan, C.; Lai, S.C.S.; Fermin, D.J.; Unwin, P.R.; Rodriguez, P. Electrochemical characterization and regeneration of sulfur poisoned Pt catalysts in aqueous media. *J. Electroanal. Chem.* **2018**, *816*, 138–148, doi:10.1016/j.jelechem.2018.03.015.

48. Oudar, J. Sulfur Adsorption and Poisoning of Metallic Catalysts. *Catal. Rev.* **1980**, *22*, 171–195, doi:10.1080/03602458008066533.

49. Truex, T.J. Interaction of sulfur with automotive catalysts and the impact on vehicle emissions-a review. *SAE Tech. Pap.* **1999**, *108*, 1192–1206, doi:10.4271/1999-01-1543.

50. Sui, S.; Wang, X.; Zhou, X.; Su, Y.; Riffat, S.; Liu, C. A comprehensive review of Pt electrocatalysts for the oxygen reduction reaction: Nanostructure, activity, mechanism and carbon support in PEM fuel cells. *J. Mater. Chem. A* **2017**, *5*, 1808–1825, doi:10.1039/C6TA08580F.

51. Luo, H.; Park, S.; Chan, H.Y.H.; Weaver, M.J. Surface Oxidation of Platinum-Group Transition Metals in Ambient Gaseous Environments: Role of Electrochemical versus Chemical Pathways. *J. Phys. Chem. B* **2000**, *104*, 8250–8258, doi:10.1021/jp001289+.

52. Pradeep, T.; Anshup Noble metal nanoparticles for water purification: A critical review. *Thin Solid Films* **2009**, *517*, 6441–6478, doi:10.1016/j.tsf.2009.03.195.

53. Goyer, R.A. Toxic And Essential Metal Interactions. *Annu. Rev. Nutr.* **1997**, *17*, 37–50, doi:10.1146/annurev.nutr.17.1.37.

54. Hodgson, A.; Haq, S. Water adsorption and the wetting of metal surfaces. *Surf. Sci. Rep.* **2009**, *64*, 381–451, doi:10.1016/j.surfrep.2009.07.001.

55. Guo, L.Q.; Zhao, X.M.; Bai, Y.; Qiao, L.J. Water adsorption behavior on metal surfaces and its influence on surface potential studied by in situ SPM. *Appl. Surf. Sci.* **2012**, *258*, 9087–9091, doi:10.1016/j.apsusc.2012.06.003.

56. Carrasco, J.; Hodgson, A.; Michaelides, A. A molecular perspective of water at metal interfaces. *Nat. Mater.* **2012**, *11*, 667–674, doi:10.1038/nmat3354.

57. Bellarosa, L.; García-Muelas, R.; Revilla-López, G.; López, N. Diversity at the water-metal interface: Metal, water thickness, and confinement effects. *ACS Cent. Sci.* **2016**, *2*, 109–116, doi:10.1021/acscentsci.5b00349.

58. Meng, S.; Wang, E.G.; Gao, S. Water adsorption on metal surfaces: A general picture from density functional theory studies. *Phys. Rev. B* **2004**, *69*, 195404, doi:10.1103/PhysRevB.69.195404.

59. Kenmoe, S.; Ulrich Biedermann, P. Water aggregation and dissociation on the ZnO(1010) surface. *Phys. Chem. Chem. Phys.* **2017**, *19*, 1466–1486, doi:10.1039/c6cp07516a.

60. Kresse, G.; Hafner, J. Ab initio molecular dynamics for liquid metals. *Phys. Rev. B* **1993**, *47*, 558–561, doi:10.1103/PhysRevB.47.558.

61. Kresse, G.; Hafner, J. Ab initio molecular-dynamics simulation of the liquid-metalamorphous-semiconductor transition in germanium. *Phys. Rev. B* **1994**, *49*, 14251–14269, doi:10.1103/PhysRevB.49.14251.

62. Kresse, G.; Furthmüller, J. Efficient iterative schemes for ab initio total-energy calculations using a plane-wave basis set. *Phys. Rev. B* **1996**, *54*, 11169–11186, doi:10.1103/PhysRevB.54.11169.

63. Kresse, G.; Furthmüller, J. Efficiency of ab-initio total energy calculations for metals and semiconductors using a plane-wave basis set. *Comput. Mater. Sci.* **1996**, *6*, 15–50, doi:10.1016/0927-0256(96)00008-0.

64. Posada-Pérez, S.; Santos-Carballal, D.; Terranova, U.; Roldan, A.; Illas, F.; de Leeuw, N.H. CO2 interaction with violarite (FeNi2S4) surfaces: a dispersion-corrected DFT study. *Phys. Chem. Chem. Phys.* **2018**, *20*, 20439–20446, doi:10.1039/C8CP03430C.

65. Dzade, N.Y.; Roldan, A.; de Leeuw, N.H. Activation and dissociation of CO 2 on the (001), (011), and (111) surfaces of mackinawite (FeS): A dispersion-corrected DFT study. *J. Chem. Phys.* **2015**, *143*, 094703, doi:10.1063/1.4929470.

66. Mishra, A.K.; Roldan, A.; de Leeuw, N.H. CuO Surfaces and CO2 Activation: A Dispersion-Corrected DFT+ U Study. *J. Phys. Chem. C* **2016**, *120*, 2198–2214, doi:10.1021/acs.jpcc.5b10431.

67. Santos-Carballal, D.; Roldan, A.; Dzade, N.Y.; de Leeuw, N.H. Reactivity of CO2 on the surfaces of magnetite (Fe3O4), greigite (Fe3S4) and mackinawite (FeS). *Philos. Trans. R. Soc. A Math. Phys. Eng. Sci.* **2018**, *376*, 20170065, doi:10.1098/rsta.2017.0065.

68. Ungerer, M.J.; Santos-Carballal, D.; Cadi-Essadek, A.; van Sittert, C.G.C.E.; de Leeuw, N.H. Interaction of H2O with the Platinum Pt (001), (011) and (111) Surfaces: A Density Functional Theory Study with Long-Range Dispersion Corrections. *J. Phys. Chem. C* **2019**, acs.jpcc.9b06136, doi:10.1021/acs.jpcc.9b06136.

69. Ungerer, M.J.; Santos-Carballal, D.; Cadi-Essadek, A.; Van Sittert, C.G.C.E.; Leeuw, N.H. de Interaction of SO2 with the Platinum (001), (011) and (111) Surfaces: A DFT Study. *Surf. Chem. Catal.* **2020**.

70. Blöchl, P.E. Projector augmented-wave method. *Phys. Rev. B* **1994**, *50*, 17953–17979, doi:10.1103/PhysRevB.50.17953.

71. Kresse, G.; Joubert, D. From ultrasoft pseudopotentials to the projector augmented-wave method. *Phys. Rev. B* **1999**, *59*, 1758–1775, doi:10.1103/PhysRevB.59.1758.

72. Perdew, J.P.; Burke, K.; Ernzerhof, M. Generalized Gradient Approximation Made Simple. *Phys. Rev. Lett.* **1996**, *77*, 3865–3868, doi:10.1103/PhysRevLett.77.3865.

73. Perdew, J.P.; Burke, K.; Ernzerhof, M. Generalized Gradient Approximation Made Simple-ERRATA. *Phys. Rev. Lett.* **1996**, *77*, 3865–3868, doi:10.1103/PhysRevLett.77.3865.

74. Grimme, S.; Ehrlich, S.; Goerigk, L. Effect of the damping function in dispersion corrected density functional theory. *J. Comput. Chem.* **2011**, *32*, 1456–1465, doi:10.1002/jcc.21759.

75. Methfessel, M.; Paxton, A.T. High-precision sampling for Brillouin-zone integration in metals. *Phys. Rev. B* **1989**, *40*, 3616–3621, doi:10.1103/PhysRevB.40.3616.

76. Blöchl, P.E.; Jepsen, O.; Andersen, O.K. Improved tetrahedron method for Brillouin-zone integrations. *Phys. Rev. B* **1994**, *49*, 16223–16233, doi:10.1103/PhysRevB.49.16223.

77. Corbel, G.; Topić, M.; Gibaud, A.; Lang, C.I. Selective dry oxidation of the ordered Pt-11.1 at.% v

alloy surface evidenced by in situ temperature-controlled X-ray diffraction. *J. Alloys Compd.* **2011**, *509*, 6532–6538, doi:10.1016/j.jallcom.2011.03.079.

78. Monkhorst, H.J.; Pack, J.D. Special points for Brillouin-zon integrations. *Phys. Rev. B* **1976**, *13*, 5188–5192, doi:10.1103/PhysRevB.16.1748.

79. Arblaster, J.W. Crystallographic properties of platinum. *Platin. Met. Rev.* **1997**, *41*, 12–21, doi:http://www.technology.matthey.com/article/41/1/12-21/.

80. Arblaster, J.W. Crystallographic properties of platinum (Errata). *Platin. Met. Rev.* **2006**, *50*, 118–119, doi:10.1595/147106706X129088.

81. Watson, G.W.; Kelsey, E.T.; de Leeuw, N.H.; Harris, D.J.; Parker, S.C. Atomistic simulation of dislocations, surfaces and interfaces in MgO. *J. Chem. Soc. Faraday Trans.* **1996**, *92*, 433, doi:10.1039/ft9969200433.

82. Lang, N.D.; Kohn, W. Theory of metal surfaces: Work function. *Phys. Rev. B* **1971**, *3*, 1215–1223, doi:10.1103/PhysRevB.3.1215.

83. Henkelman, G.; Arnaldsson, A.; Jónsson, H. A fast and robust algorithm for Bader decomposition of charge density. *Comput. Mater. Sci.* **2006**, *36*, 354–360, doi:10.1016/j.commatsci.2005.04.010.

84. Sanville, E.; Kenny, S.D.; Smith, R.; Henkelman, G. Improved grid-based algorithm for Bader charge allocation. *J. Comput. Chem.* **2007**, *28*, 899–908, doi:10.1002/jcc.20575.

85. Tang, W.; Sanville, E.; Henkelman, G. A grid-based Bader analysis algorithm without lattice bias. *J. Phys. Condens. Matter* **2009**, *21*, 084204, doi:10.1088/0953-8984/21/8/084204.

86. Yu, M.; Trinkle, D.R. Accurate and efficient algorithm for Bader charge integration. *J. Chem. Phys.* **2011**, *134*, 1–8, doi:10.1063/1.3553716.

87. Skriver, H.L.; Rosengaard, N.M. Surface energy and work function of elemental metals. *Phys. Rev. B* **1992**, *46*, 7157–7168, doi:10.1103/PhysRevB.46.7157.

88. De Leeuw, N.H.; Nelson, C.J. A computer modeling study of perfect and defective silver (111) surfaces. *J. Phys. Chem. B* **2003**, *107*, 3528–3534, doi:10.1021/jp027001t.

89. Singh-Miller, N.E.; Marzari, N. Surface energies, work functions, and surface relaxations of low-index metallic surfaces from first principles. *Phys. Rev. B - Condens. Matter Mater. Phys.* **2009**, *80*, doi:10.1103/PhysRevB.80.235407.

90. Jian-Min, Z.; Fei, M.; Ke-Wei, X. Calculation of the surface energy of fcc metals with modified embedded-atom method. *Chinese Phys.* **2004**, *13*, 1082–1090, doi:10.1088/1009-1963/13/7/020.

91. Keene, B.J. Review of data for the surface tension of pure metals. *Int. Mater. Rev.* **1993**, *38*, 157–192, doi:10.1179/imr.1993.38.4.157.

92. Tyson, W.R.; Miller, W.A. Surface free energies of solid metals: Estimation from liquid surface tension measurements. *Surf. Sci.* **1977**, *62*, 267–276, doi:10.1016/0039-6028(77)90442-3.

93. Xin, H.; Linic, S. Communications: Exceptions to the d -band model of chemisorption on metal surfaces: The dominant role of repulsion between adsorbate states and metal d -states. *J. Chem. Phys.* **2010**, *132*, doi:10.1063/1.3437609.

94. Caglar, B.; Kizilkaya, A.C.; Niemantsverdriet, J.W. (Hans); Weststrate, C.J. (Kees-J. Application of work function measurements in the study of surface catalyzed reactions on Rh(1 0 0). *Catal. Struct. React.* **2018**, *4*, 1–11, doi:10.1080/2055074X.2018.1434986.

95. Norskov, J.K.; Abild-Pedersen, F.; Studt, F.; Bligaard, T. Density functional theory in surface chemistry and catalysis. *Proc. Natl. Acad. Sci.* **2011**, *108*, 937–943, doi:10.1073/pnas.1006652108.

96. Hoy, A.R.; Bunker, P.R. A precise solution of the rotation bending Schrödinger equation for a triatomic molecule with application to the water molecule. *J. Mol. Spectrosc.* **1979**, *74*, 1–8, doi:10.1016/0022-2852(79)90019-5.

97. Tromp, R.H.; Postorino, P.; Neilson, G.W.; Ricci, M.A.; Soper, A.K. Neutron diffraction studies of H2O/D2O at supercritical temperatures. A direct determination of g HH (r), g OH (r), and g OO (r). *J. Chem. Phys.* **1994**, *101*, 6210–6215, doi:10.1063/1.468403.

98. Clark, A.H.; Beagley, B. Electron-diffraction investigations of gaseous sulphur dioxide and trioxide. *Trans. Faraday Soc.* **1971**, *67*, 2216, doi:10.1039/tf9716702216.

99. Thiel, P.A.; Madey, T.E. The interaction of water with solid surfaces: Fundamental aspects. *Surf. Sci. Rep.* **1987**, *7*, 211–385, doi:10.1016/0167-5729(87)90001-X.

100. Henderson, M. The interaction of water with solid surfaces: fundamental aspects revisited. *Surf. Sci. Rep.* **2002**, *46*, 1–308, doi:10.1016/S0167-5729(01)00020-6.

101. Feibelman, P.J. Partial Dissociation of Water on Ru(0001). *Science (80-.).* **2002**, *295*, 99–102, doi:10.1126/science.1065483.

102. Ludwig, R. How Does Water Bind to Metal Surfaces: Hydrogen Atoms Up or Hydrogen Atoms Down? *Angew. Chemie Int. Ed.* **2003**, *42*, 3458–3460, doi:10.1002/anie.200301658.

103. Kubas, G.J. Diagnostic Features of Transition-Metal-S02 Coordination Geometries. *Inorg. Chem.* **1979**, *18*, 182.

104. Benedict, W.S.; Gailar, N.; Plyler, E.K. Rotation-Vibration Spectra of Deuterated Water Vapor. *J. Chem. Phys.* **1956**, *24*, 1139–1165, doi:10.1063/1.1742731.

105. Jirsak, T.; Rodriguez, J.A.; Chaturvedi, S.; Hrbek, J. Chemistry of SO2 on Ru(001): formation of SO3 and SO4. *Surf. Sci.* **1998**, *418*, 8–21, doi:10.1016/S0039-6028(98)00652-9.

106. Shi, Q.; Sun, R. Adsorption manners of hydrogen on Pt(1 0 0), (1 1 0) and (1 1 1) surfaces at high coverage. *Comput. Theor. Chem.* **2017**, *1106*, 43–49, doi:10.1016/j.comptc.2017.02.024.

107. Haase, J. Structural studies of SO2 adsorption on metal surfaces. *J. Phys. Condens. Matter* **1997**, *9*, 3647–3670, doi:10.1088/0953-8984/9/18/006.

108. Carrasco, J.; Klimeš, J.; Michaelides, A. The role of van der Waals forces in water adsorption on metals. *J. Chem. Phys.* **2013**, *138*, doi:10.1063/1.4773901.

109. Michaelides, A.; Ranea, V.A.; de Andres, P.L.; King, D.A. General Model for Water Monomer Adsorption on Close-Packed Transition and Noble Metal Surfaces. *Phys. Rev. Lett.* **2003**, *90*, 216102, doi:10.1103/PhysRevLett.90.216102.

110. Happel, M.; Luckas, N.; Viñes, F.; Sobota, M.; Laurin, M.; Libuda, J. SO2 Adsorption on Pt(111) and Oxygen Precovered Pt(111): A Combined Infrared Reflection Absorption Spectroscopy and Density Functional Study. *J. Phys. Chem. C* **2011**, *115*, 479–491, doi:10.1021/jp107171t.

111. Ryan, R.R.; Kubas, G.J.; Moody, D.C.; Eller, P.G. Structure and bonding of transition metal-sulfur dioxide complexes. In *Structural Bonding*; 1981; Vol. 46, pp. 47–100.